Available online at www.sciencedirect.com
SCIENCE DIRECT®
Biochimica et Biophysica Acta 1660 (2004) 80–92
BIOCHIMICA ET BIOPHYSICA ACTA
BBA
www.bba-direct.com

Stability and solubility of integral membrane proteins from photosynthetic bacteria solubilized in different detergents

Takayuki Odahara*

National Institute of Advanced Industrial Science and Technology (AIST), Tsukuba Central-6, 1-1 Higashi, Tsukuba, Ibaraki 305-8566, Japan

Received 24 April 2003; received in revised form 17 October 2003; accepted 4 November 2003

Abstract

As a first step toward the establishment of practical guidelines for the search for crystallization conditions, stability and solubility were examined for integral membrane proteins from photosynthetic bacteria in the presence of different detergents. The results obtained from their stability provided practical information on the proper choice of detergent type in the preparation process and the subsequent crystallization experiment. In addition, the determination of a solubility diagram provided a practical method for quantifying the correct choice of detergent concentration and for setting up the suitable precipitant concentration in the crystallization experiment.

Keywords: Solubility diagram; Integral membrane protein; Detergent; Amorphous precipitate; Crystal

1. Introduction

An integral membrane protein has both distinct hydrophobic and hydrophilic regions on its surface. To solubilize and purify such an amphiphilic protein with its native conformation in an aqueous solution, it is necessary to cover its hydrophobic surface with suitable small amphiphilic molecules, detergents. Detergent molecules binding to the convoluted hydrophobic surface reduce the possibility that a protein–detergent complex will crystallize. In addition, the combination of factors (such as detergent type, detergent concentration, salt type, salt concentration, precipitant type, precipitant concentration, temperature and pH of solvent), which seem to affect the crystallization of a complex, is so varied that an empirical and exhausting search for its crystallization conditions requires a large amount of the protein.

Many solubilized protein–detergent complexes have been crystallized by orthodox methods [1,2] during the 20 years since the first successes [3–6]. However, the accumulation of their crystallization conditions is rather small and the appreciation of their behavior in an aqueous solution is insufficient compared with aqueous-soluble proteins [7,8]. Thus, the crystallization of the complex remains the most intimidating and risky step in X-ray crystallography.

In order to overcome such a difficult situation, it is necessary to derive useful features common to successful crystallization conditions in advance, through systematical examination of the property and behavior of complexes. Firstly, for the choice of suitable detergents in solubilization and crystallization steps, stability was examined for integral membrane proteins from photosynthetic bacteria in the presence of individual different detergents. Secondly, for setting up suitable precipitant concentration in a crystallization trial, solubility diagrams [9–12] were determined for different complexes and the protein solubility was compared with crystallization features. Lastly, the influence of deter-

Abbreviations: Brij-35, polyoxyethylene lauryl alcohol ether; $C_{12}E_8$, polyoxyethylene 8 lauryl ether; Triton X-100, t-octylphenoxypolethoxyethanol; DDAO, *n*,*n*-dimethyldecylamine-*n*-oxide; LDAO, *n*,*n*-dimethyldodecylamine-*n*-oxide; OG, *n*-octyl-β-D-glucoside; SB-12, *n*-dodecyl-*n*,*n*-dimethyl-3-ammonio-1-propanesulfate; MEGA-9, nonanoyl-*n*-methylglucamide; MEGA-10, decanoyl-*n*-methylglucamide; HTG, *n*-heptyl-β-D-thioglucoside; OTG, *n*-octyl-β-D-thioglucoside; SM-1000, β-D-fructopyranosyl-α-D-glucopyranoside monodecanoate; SM-1200, β-D-fructopyranosyl-α-D-glucopyranoside monododecanoate; OM, *n*-octyl-β-D-maltopyranoside; DM, *n*-decyl-β-D-maltopyranoside; LM, *n*-dodecyl-β-D-maltopyranoside; NTM, *n*-nonyl-β-D-thiomaltoside; CHAPS, 3-[(3-cholamidopropyl) dimethylammonio]-1-propanesulfonate; SC, sodium cholate; SDC, sodium deoxycholate; DOPC, L-a-dioctanoyl phosphatidylcholine; Tris, Tris(hydroxymethyl)aminomethane hydrochloride; EDTA-2Na^+, disodium ethylenediaminetetraacetate; NaN_3, sodium azide; PEG, polyethylene glycol

* Tel.: +81-29-861-6182; fax: +81-29-861-6182.
E-mail address: odahara-takayuki@aist.go.jp (T. Odahara).

0005-2736/$ - see front matter © 2003 Elsevier B.V. All rights reserved.
doi:10.1016/j.bbamem.2003.11.003

gent concentration and type on protein solubility was examined for two different proteins using polyethylene glycol (PEG) 4000 and ammonium sulfate as precipitants.

2. Materials and methods

2.1. Preparation of integral membrane proteins from photosynthetic bacteria

Rhodobacter sphaeroides RC, *Rhodopseudomonas viridis* RC, *Rb. sphaeroides* B800–850 and *Rhodobacter capsulatus* B800–850 were solubilized from their respective purified photosynthetic membranes, using purified *n*,*n*-dimethyldodecylamine-*n*-oxide (LDAO) given by Lion Corporation. The purification of each protein was carried out using a phenyl-Toyopearl 650 hydrophobic column (Tosoh) and/or CL-6B molecular sieve chromatography (Pharmacia) in addition to the reported methods [13–17]. *Rp. viridis* RC-B1020 and *Rhodospirillum rubrum* RC-B890 were solubilized in 3-[(3-cholamidopropyl) dimethylammonio]-1-propanesulfonate (CHAPS, Dojindo) and the mixture of cholate (Wako Pure Chemical Industries) and deoxycholate (Wako), respectively, and purified according to the reported methods [18,19]. Tris buffer solution (10 mM Tris(hydroxymethyl)aminomethane hydrochloride (Tris, Sigma)–HCl, 1 mM disodium ethylenediaminetetraacetate (EDTA-2Na$^+$, Dojindo) and 0.02% (w/v) sodium azide (NaN_3, Wako) pH 8.0) containing each solubilization detergent was used at all the purification steps. In order to avoid instability of the proteins, a detergent concentration higher than each CMC was used in all the preparation steps. Once obtained, those complexes were free of contaminating polypeptides on SDS polyacrylamide gels (ATTO Corporation, PAGEL AE-6000).

2.2. Test of stability in different detergents

The sample solutions were concentrated up to about 50 mg/ml in an ultrafiltration apparatus employing an ADVANTEC UK-200 membrane of which the molecular weight limit is 200 kDa. To reduce the amount of a solubilization detergent brought to the new detergent/buffer solution, 6 μl of the protein solution was individually dispersed into 3 ml of Tris buffer solution containing a required detergent. The protein solutions were incubated at 4 °C in the dark. The stability of each integral membrane protein was determined from the time dependence of their absorption spectra.

2.3. Replacement of detergent and buffer solution

Purified proteins were individually absorbed to a DEAE-Sephacel (Pharmacia) anion exchange column which was previously equilibrated with Tris buffer solution containing the detergent used for solubilization, washed with at least 10 times column volume of the same buffer solution containing a required detergent, and then eluted with the same medium with 300 mM NaCl. For the replacement of buffer solution, each protein was filtered on a Sephadex G-25 (Pharmacia) column which was previously equilibrated with required detergent/buffer solution. To replace them completely without the condensation of detergent micelles, each sample solution was further washed five to eight times with the required solution in the ultrafiltration apparatus above.

2.4. Solubility measurements and crystallization

Solutions of twice the desired PEG4000 (Merck) or ammonium sulfate ($(NH_4)_2SO_4$) (Wako) concentration were prepared in a required buffer solution. A sample solution of twice the desired protein concentration (20–30 mg/ml) was mixed with an equal volume of the precipitant solution in a small test tube (0.5 ml) on a vortex mixer. After an amorphous precipitate was removed from the solution by centrifugation at 12,000 rpm (Hitachi T15AP21) for 6 min, the protein concentration in the supernatant was determined photometrically by measuring the absorbance at a peak characteristic of each protein. Such a procedure was carried out at 21–23 °C, and all the measurements were completed within 15 min of mixing. The same stock solutions of chemicals were used consistently for the preparation of sample and precipitant solutions. Concentrations of *Rb. sphaeroides* RC [20], *Rp. viridis* RC [13,21], *Rb. sphaeroides* B800–850, *Rb. capsulatus* B800–850 [17] and *Rp. viridis* RC-B1020 [18] were based on the relationship where one unit at 800, 830, 800, 800 and 1020 nm corresponds to 0.33, 0.45, 0.083, 0.083 and 0.086 mg/ml of the proteins, respectively. Samples with $A_{280}/A_{800} \leq 1.4$, $A_{280}/A_{830} \leq 2.6$, $A_{280}/A_{850} \leq 0.4$, $A_{280}/A_{850} \leq 0.4$ and $A_{280}/A_{1020} \leq 0.9$ were used for the solubility determination of *Rb. sphaeroides* RC, *Rp. viridis* RC, *Rb. sphaeroides* B800–850, *Rb. capsulatus* B800–850 and *Rp. viridis* RC-B1020, respectively.

In a crystallization experiment using the batch method, 200 μl of the supernatant set in a small test tube with a sealed cap was incubated at 25 °C in the dark. The solubility of a crystal was determined for the solution phase equilibrated with the crystalline phase in the same way. In a crystallization experiment using sitting drop vapor diffusion, 25 μl of protein droplets was set against 1 ml of reservoir solution with high precipitant concentration.

2.5. X-ray diffraction experiment

A crystal was introduced into a 0.5 ϕ thin-walled glass capillary. Intensity data were collected via monochromatized X-rays of 1.0 Å at the Photon Factory, Tsukuba, Japan, by means of a modified Weissenberg camera for macromolecules [22]. The sample-to-imaging plate distance was 286.5 mm and the exposure time for each measurement was

1 min. Diffraction intensities were processed with the program DENZO [23].

3. Results

3.1. Stability of integral membrane proteins from photosynthetic bacteria in different detergents

To ascertain the influence of detergent type on the physical stability of integral membrane proteins, change in the absorption spectra was examined for seven different pigment-containing proteins from photosynthetic bacteria in the presence of 19 individual different detergents. The results are summarized in Table 1. *Rp. viridis* RC, *Rb. sphaeroides* RC, *Rb. sphaeroides* B800–850 and *Rb. capsulatus* B800–850, which consist of several subunits interacting with each other directly within each protein, were stable in most of the detergents. This result suggests that the action of those detergents is not so strong as to disturb the interactions between subunits. On the other hand, extensive change in the absorption peak from light-harvesting pigment–protein complex Is (LH-1s) was observed for *Rp. viridis* RC-B1020 and *Rs. rubrum* RC-B850 depending on the detergent type sensitivity. The difference in the change is thought to represent the ability of detergent molecules to replace lipid molecules because LH-1s attach to a RC through lipid molecules within both proteins [24,25].

To determine the ability more quantitatively, time dependence of absorption spectrum was examined for *Rp. viridis* RC-B1020 after dispersing the protein/0.5% CHAPS solution (w/v) into Tris buffer solution containing each required detergent of high concentration (0.5–1.2% (w/v)). The relative intensity of the absorbance at 1020 nm was plotted as a function of time in Fig. 1. The decay in the absorbance increased in the order 0.5% (w/v) CHAPS (Dojindo), 0.5% (w/v) *n*-nonyl-β-D-thiomaltoside (NTM, Dojindo), 0.5% (w/v) β-D-fructopyranosyl-α-D-glucopyranoside monodecanoate (SM-1000, Dojindo), 0.7% (w/v) sodium cholate (SC, Wako), 0.5% (w/v) *n*-decyl-β-D-maltopyranoside (DM, Calbiochem), 0.5% (w/v) sodium deoxycholate (SDC, Wako), 0.5% (w/v) *n*-octyl-β-D-thioglucoside (OTG, Dojindo), 1.0% (w/v) nonanoyl-*n*-methylglucamide (MEGA-9, Dojindo), 0.5% (w/v) *n*-dodecyl-β-D-maltopyranoside (LM, Calbiochem), 1.2% (w/v) *n*-octyl-β-D-maltopyranoside (OM, Sigma), 0.5% (w/v) β-D-fructopyranosyl-α-D-glucopyranoside monododecanoate (SM-1200, Dojindo), 1.0% (w/v) L-a-dioctanoyl phosphatidylcholine (DOPC, Sigma), 0.5% (w/v) polyoxyethylene 8 lauryl ether ($C_{12}E_8$, Sigma), 0.5% (w/v) t-octylphenoxypolethoxyethanol (Triton X-100, Sigma), 1.0% (w/v) *n*-octyl-β-D-glucoside (OG, Dojindo), 0.5% (w/v) polyoxyethylene lauryl alcohol ether (Brij-35, Nacalai Tesque), 0.5% (w/v) *n*,*n*-dimethyldecylamine-*n*-oxide (DDAO, Fluka), 0.5% (w/v) LDAO (Sigma), and 0.5% (w/v) *n*-dodecyl-*n*,*n*-dimethyl-3-ammonio-1-propanesulfate (SB-12, Sigma). This sequence shows that small flexible detergents with a hydrophilic head of large polarity strongly influence the conformation of LH-1 and easily replace lipids. Such a tendency corresponded

Table 1
Stability of integral membrane proteins from photosynthetic bacteria in different detergents

Detergent	Concentration (%) (w/v)	*Rp. viridis* RC-B1020	*Rs. rubrum* RC-B890	*Rp. viridis* RC	*Rb. sphaeroides* RC	*Rb. capsulatus* RC	*Rb. sphaeroides* B800–850	*Rb. capsulatus* B800–850
SB-12	0.5	–	–	+	+	+	+	+
SB-14	0.5	–	–	+	+	+	+	+
$C_{12}E_8$	0.5	–	–	+	+	+	+	+
Brij-35	0.5	–	–	+	+	–	±	+
Triton X-100	0.5	±	±	+	+	+	+	+
DDAO	0.5	–	–	+	+*	+	+	+
LDAO	0.5	–	–	+	+	+	+	+
MEGA-9	1.0	+	+	+	+	+	+	+
MEGA-10	0.5	±	±	+	+	+	+	+
OG	1.0	–	–	+*	+	+	+	+
HTG	1.0	±	±	+	+	+	+	+
OTG	0.5	+	+	+	+	+	+	+
SM-1000	0.5	+	+	+	+	+	+	+
SM-1200	0.5	±	+	+	+	+	+	+
DM	0.5	+	+	+	+	+	+	+
LM	0.5	+	+	+	+	+	+	+
CHAPS	0.5	+	+	+	+	+	+	+
SC	1.0	+	+	+	+	+	+	+
SDC	0.5	+	+	+	+	+	+	+

(+) Stable (>90%); (±) slightly denatured (90–50%); (–) denatured (50%>) in the presence of 10 mM Tris–HCl (pH 8.0), 1 mM EDTA-2Na^+ and 0.02% (w/v) NaN_3.

* Although *Rp. viridis* RC and *Rb. sphaeroides* RC gradually precipitated in the presence of OG and DDAO, respectively, spectra of those precipitates resuspended in Tris buffer solutions containing 0.1% (w/v) LDAO were no different from those of natural ones.

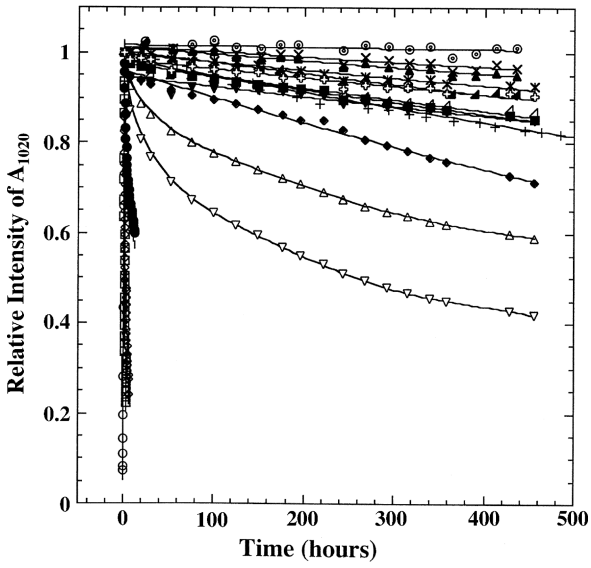

Fig. 1. Time dependence of absorbance at 1020 nm of *Rp. viridis* RC-1020 in the presence of different detergents at 4 °C. The concentrations and types of detergents used were: 0.5% (w/v) LDAO (○), 0.5% (w/v) DDAO (□), 0.5% (w/v) Brij-35 (◇), 0.5% (w/v) $C_{12}E_8$ (△), 0.5% (w/v) Triton X-100 (▽), 1.0% (w/v) MEGA-9 (⊿), 1.0% (w/v) OG (●), 0.5% (w/v) OTG (■), 0.5% (w/v) SM-1200(◆), 0.5% (w/v) SM-1000 (▲), 0.5% (w/v) LM (▼), 0.5% (w/v) DM (◢), 1.2% (w/v) OM (+), 0.5% (w/v) NTM (×), 0.5% (w/v) CHAPS (◎), 0.7% (w/v) SC (∗), 0.5% (w/v) SDC (⇧). The other conditions were: 10 mM Tris–HCl (pH 8.0), 0.02% (w/v) NaN_3 and 1 mM EDTA-$2Na^+$.

well with that from thermal stability of rhodopsin and opsin [21,26]. Both results are summarized in Table 2. In addition, this protein was most stable in a 10-carbon alkyl tail detergent among the same hydrophilic head. This result is related to the width of cylindrical hydrophobic surface of the protein.

Stability was also examined for *Rp. viridis* RC-B1020 dispersed into Tris buffer solution containing a required detergent of slightly higher concentration than each CMC. For 0.2% (w/v) SM-1000, 0.1% (w/v) SM-1000, 0.1% (w/v) DM and 0.1% (w/v) LM, the absorbance at 1020 nm decayed more rapidly than the result shown in Fig. 1. Such influence of low detergent concentration would be ascribed to the release of CHAPS molecules from the hydrophobic surface of the protein because the CHAPS concentration was suddenly diluted to below its CMC (0.49% (w/v)) immediately after dispersing. Thus, we must be careful of not only the type but also the concentration of the detergent replacement.

3.2. Determination of solubility diagram and crystallization of integral membrane proteins

To appreciate the relationship between the solubility of a protein–detergent complex and the precipitant concentration suitable for inducing a protein crystal, we determined a solubility diagram for three different integral membrane proteins (*Rb. sphaeroides* RC, *Rp. viridis* RC and *Rb. capsulatus* B800–850). Chemicals and pH used in initial crystallization experiments [14,17,27–30] were also adopted in this experiment. Upon the addition of a sufficient amount of precipitant, reflecting the variety of nonspecific interaction between complexes in site and manner, an amorphous precipitate of the complex formed instantaneously. After removing the precipitate by centrifugation, the protein concentration in the supernatant was immediately determined. For *Rb. sphaeroides* RC solubilized in LDAO and OG (Fig. 2A), *Rb. capsulatus* B800–850 in LDAO and *Rp. viridis* RC in LDAO (Fig. 2B), the protein concentration decreased steeply with an increase of PEG4000 concentration above 15%, 10% and 11% (w/v) and of $(NH_4)_2SO_4$ concentration above 21% (w/v), respectively. The result obtained for *Rb. sphaeroides* RC/LDAO complex consist of data measured for four different preparations. Those data agreed with each other to within 1% (w/v) with respect to PEG4000 concentration. In addition, the protein concentration (S) remaining in supernatant solution at a given precipitant concentration (P) was given by

$$S = Ae^{-BP}, \quad (1)$$

where A and B are constants [11,31].

From such a clear relationship and good reproducibility, although a solution phase is not equilibrated with an amorphous precipitate, in this study we define solubility of an amorphous precipitate (precipitate solubility) as concentration of a protein remaining in solution immediately after an amorphous precipitate separates from a solution phase. Solubility curves for an amorphous precipitate (precipitate

Table 2
Effect of detergent type on physical stability of *Rp. viridis RC*-B1020

harsh ⇐						⇒ mild	
SB-12 > LDAO > DDAO > Brij-35 > OG > Triton X-100 > NG > C12E8 > SM-1200 > HTG > OM, LM > DM > SM-1000 > NTM > CHAPS OTG > SC MEGA-9 > SDC							
LDAO	>	OG > SB-12>SB-14	> NG>Triton X-100		> DG > DM	> LM	Ref. [21, 26]

curves) were obtained by least-squares fitting of Eq. (1) to the precipitate solubility at each precipitant concentration. Protein concentration obtained at low precipitant concentration was lower than that estimated from the precipitate curves. This is because an excessive amount of amorphous precipitates was induced by the contact of highly concentrated protein and precipitant solutions at the beginning of mixing. Such a tendency is usually enhanced by an increase in starting protein concentration.

Protein-rich and protein-poor phases [32] were observed in the supernatant solutions of *Rb. sphaeroides* RC and *Rb. capsulatus* B800–850 in a few hours; such phase separation is usually promoted by multivalent ions, basic pH and a high temperature above 25 °C. Crystals formed in the protein-rich phase, and the phase separation decreased with crystal growth. For *Rb. sphaeroides* RC solubilized in LDAO and OG, *Rb. capsulatus* B800–850 in LDAO and *Rp. viridis* RC in LDAO, crystals formed finally in the range of 15.5–24.5%, 10–19.5%, 11–13% (w/v) PEG4000 and 20.5–26.5% (w/v) $(NH_4)_2SO_4$, respectively. With an increase in precipitant concentration, the time it took for the appearance of crystals decreased, the total number of crystals increased and the size decreased. Protein concentration in each sample solution was determined again 1 month after the preparation, a period sufficient for the phase equilibrium between solution and crystal [11,12]. Since the protein concentration also decreased clearly in a single exponential way with an increase in precipitant concentration [11,12], solubility curves of crystals were determined as well as precipitate curves. All the solubility curves were located below the corresponding precipitate curves on the diagram. This result means that the specific interaction necessary for inducing the crystallization is stronger than nonspecific interactions. In addition, the slopes of solubility curves, B in Eq. (1), were the same as, or steeper than those of corresponding precipitate curves, maybe due to the more homogeneous property of the specific interaction. As shown in Fig. 3A, this result leads to the relationship where the degree of supersaturation, a driving force of crystal growth, increases with an increase in precipitant concentration. At the same time, there is a precipitant concentration giving the maximum amount of protein converted to crystalline phase as shown in Fig. 3B. Such tendencies are also well reflected in the features observed in crystallization of those proteins described above.

Furthermore, from the X-ray diffraction images, crystals of *Rb. sphaeroides* RC solubilized in OG and LDAO were identified to be of the same space group ($P2_12_12_1$) with

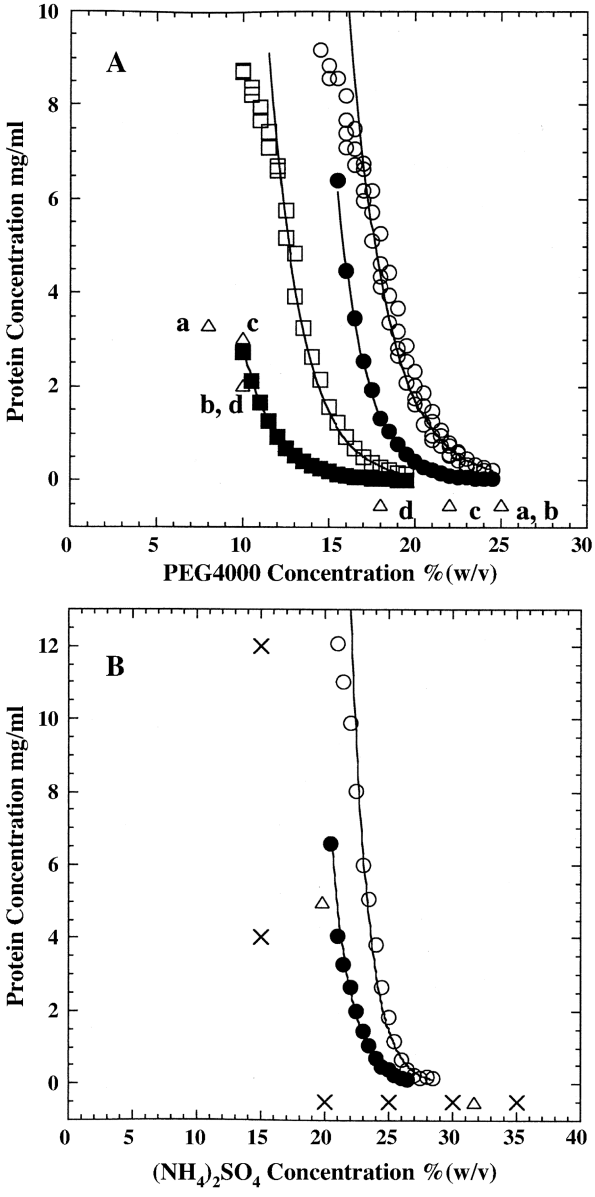

Fig. 2. Solubility diagrams of *Rb. sphaeroides* RC and *Rp. viridis* RC. (A) Solubility diagram of *Rb. sphaeroides* RC as a function of PEG4000 concentration. The symbols are open circles, precipitate solubility in the presence of 0.1% (w/v) LDAO at 23 °C; and open squares, in the presence of 0.8% (w/v) OG at 23 °C. The corresponding filled symbols are crystal solubility at 25 °C. Precipitate curves in the presence of LDAO and OG were obtained by least-squares fitting of a single exponential function to the protein solubility in the range of 16–24.5% and 11.5–19.5% (w/v) PEG4000, respectively. Solubility curves in the presence of LDAO and OG were obtained by least-squares fitting of a single exponential function to the protein solubility in the range of 15.5–24.5% and 10–19.5% (w/v) PEG4000, respectively. The other conditions were: 10 mM Tris–HCl (pH 8.0), 1 mM EDTA-$2Na^+$, 0.02% (w/v) NaN_3 and 300 mM NaCl. The initial conditions (△) of the sample and reservoir solution in the previous vapor diffusion experiments (a, Ref. [20]; b, Ref. [28]; c, Ref. [14]; and d, Ref. [30]) are inserted in this diagram. (B) Solubility diagram of *Rp. viridis* RC as a function of $(NH_4)_2SO_4$ concentration. The symbols are open circles, precipitate solubility at 23 °C; and filled circles, crystal solubility at 25 °C. Precipitate and solubility curves were obtained by least-squares fitting of a single exponential function to the protein solubility in the range of 22–27.5% and 20.5–26.5% (w/v) $(NH_4)_2SO_4$, respectively. The other conditions were: 100 mM sodium phosphate (pH 7.0), 1 mM EDTA-$2Na^+$, 0.02% (w/v) NaN_3, 3% (w/v) triethylammonium phosphate, 3% (w/v) 1,2,3-heptanetriol and 0.5% (w/v) LDAO. The initial conditions of the sample and reservoir solution in this study are represented by crosses (see Fig. 4). The initial condition (△) of the sample and reservoir solutions in the previous vapor diffusion experiment [27] are also inserted in this diagram.

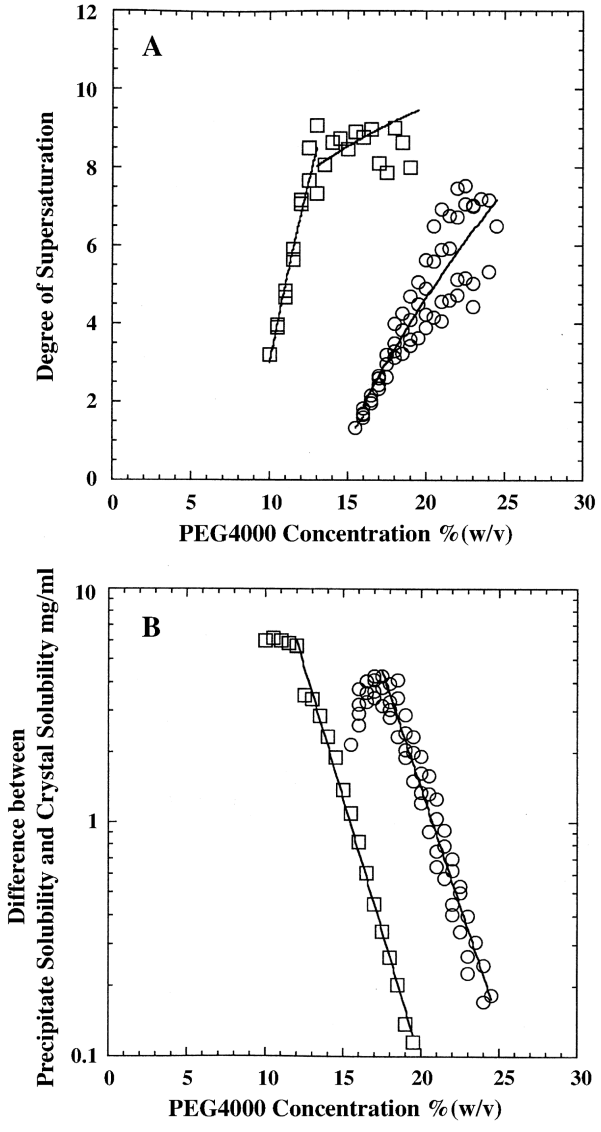

Fig. 3. PEG4000 concentration dependence of degree of supersaturation and the amount of protein converted to crystalline phase of *Rb. sphaeroides* RC. (A) The ratio of precipitate solubility to crystal solubility is plotted as a function of PEG4000 concentration. (B) Difference between precipitate solubility and crystal solubility is plotted as a function of PEG4000 concentration in a semi-logarithmic way. The concentrations and types of solubilization detergents were: 0.8% (w/v) OG (○) and 0.1% (w/v) LDAO (□). The other conditions were: 10 mM Tris–HCl (pH 8.0), 1 mM EDTA-$2Na^+$, 0.02% (w/v) NaN_3 and 300 mM NaCl.

similar unit cell dimensions (a = 141.8–142.2 Å, b = 138.0–139.6 Å and c = 77.5–78.7 Å), which correspond well with the results reported for the crystals of *Rb. sphaeroides* (wild-type and carotenoid-less mutant) RC [14,28–30]. These results mean that interaction sites between the protein molecules are the same in both crystals [33]. However, it is evident from Fig. 2A that the intensity of the protein–protein interactions varies depending on the property of micelle surface. Therefore, suitable precipitant concentration should be individually chosen, corresponding to the solubility of each target complex.

It is also necessary to clarify the relationship between the precipitate or crystal solubility and a suitable precipitant concentration in a vapor diffusion experiment because this method has been most commonly used for recent protein crystallization. Crystallization conditions adopted in the previous study [14,27–30] are also included in Fig. 2 for comparison. In those experiments, initial conditions of the sample solutions were set just below corresponding precipitate curves, and precipitant concentration in the reservoir solutions in a wide range from 18% to 25% (w/v). To establish such a relationship in more detail, different combinations of sample and reservoir conditions were applied to the crystallization of the three integral membrane proteins above. Photographs of *Rp. viridis* RC solutions at an equilibrium state, which showed the most distinctive features of all, are shown in Fig. 4. Sample solutions adjusted to the protein concentration of 12 mg/ml and the $(NH_4)_2SO_4$ concentration of 18% (w/v) were set against reservoir solutions containing 20%, 25%, 30%, 35% and 40% (w/v) $(NH_4)_2SO_4$. These conditions are also included in Fig. 2B. No crystal formed in a sample solution equilibrated with 20% (w/v) $(NH_4)_2SO_4$. As shown in Fig. 4A, B and C, with an increase of $(NH_4)_2SO_4$ concentration in the reservoir solution, crystal formation was suppressed, the amount of an amorphous precipitate increased simultaneously, and a merely amorphous precipitate formed above 35% (w/v). Such a feature is ascribed to the increase of $(NH_4)_2SO_4$ concentration in reservoir solutions, making the water evaporation from the sample solution faster than the crystal growth. In addition, when a sample solution with 4 mg/ml of protein and 18% (w/v) of $(NH_4)_2SO_4$ was equilibrated with 25% (w/v) of $(NH_4)_2SO_4$, larger crystals formed with small amounts of amorphous precipitates as shown in Fig. 4D. Such a tendency is ascribed to crystal nucleation, a well organized assembly of the complexes [34–36], which is reflected in a reduction in the number of crystals at low protein concentration. For *Rb. sphaeroides* RC and *Rb. capsulatus* B800–850, on the other hand, an increase of PEG4000 concentration in reservoir solutions led to numerous tiny crystals unlike *Rp. viridis* RC. Such a difference can be attributed to the water evaporation rate, dependent on precipitant type. Namely, the water evaporation from PEG-containing solution progresses far more slowly than that from $(NH_4)_2SO_4$-containing solution [37,38]. Therefore, the concentration of highly soluble salts such as $(NH_4)_2SO_4$ should be more carefully chosen than that of highly soluble polymers such as PEG4000.

3.3. Influence of detergent concentration on solubility and crystallization

To establish the influence of detergent concentration on the solubility and crystallization of a protein–detergent complex, precipitate and solubility curves were deter-

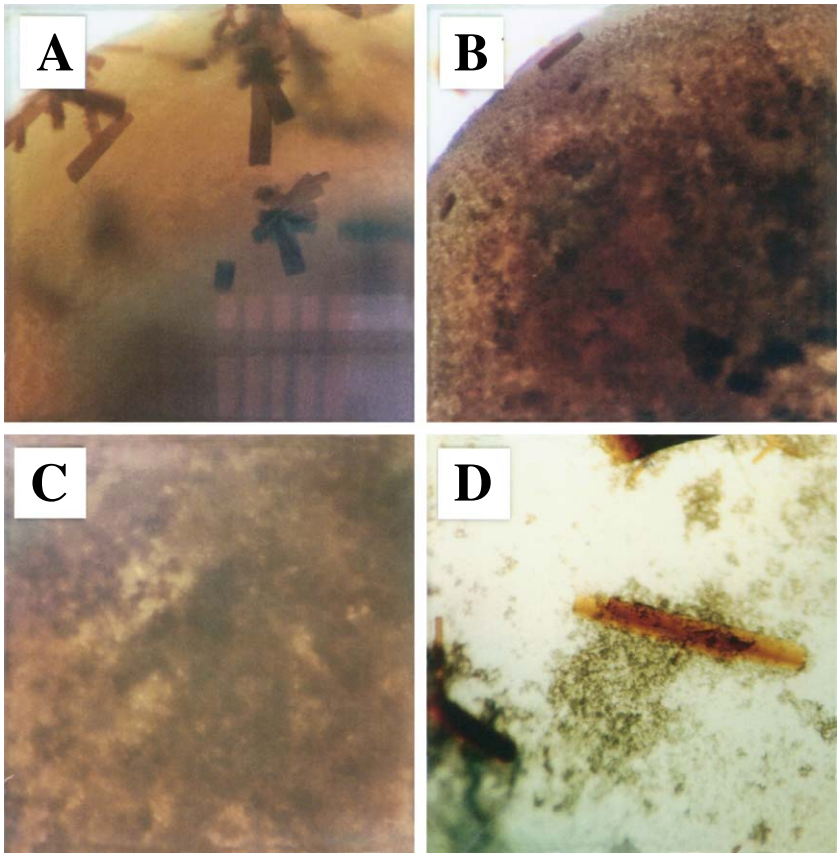

Fig. 4. Photographs of *Rp. viridis* RC reflecting the solution conditions in the vapor diffusion experiment. Initial protein concentrations of sample solutions: were 12 (A, B and C) and 4 mg/ml (D). Initial $(NH_4)_2SO_4$ concentration of sample solutions was: 15% (w/v). Initial $(NH_4)_2SO_4$ concentrations of reservoir solutions was: 25 (A and D), 30 (B) and 35% (w/v) (C). The other conditions were: 100 mM sodium phosphate (pH 7.0), 3% (w/v) triethylammonium phosphate, 3% (w/v) heptane-1,2,3-triol, 0.02% (w/v) NaN_3 and 1 mM EDTA-$2Na^+$.

mined for *Rb. sphaeroides* RC (Fig. 5A), *Rb. capsulatus* B800–850 and *Rp. viridis* RC (Fig. 5B) at different concentrations of the detergents above. The increase in the detergent concentration above each CMC barely influenced solubility. In addition, the analysis of X-ray diffraction images for obtained crystals showed no difference in crystal form or quality. Both results correspond well with a detergent phenomenon in which the amount of detergent binding to the hydrophobic surface of an integral membrane protein is relatively constant above the CMC [1]. However, the high concentration of the detergent reduced the crystallization of *Rb. sphaeroides* RC and *Rp. viridis* RC. Namely, *Rb. sphaeroides* RC formed no crystal in one-third and one-half of the sample solutions in the presence of 2.4% and 3.2% (w/v) OG, respectively, and no crystal of *Rp. viridis* RC was observed in some sample solutions in the presence of 2% (w/v) LDAO. Such a lack of reproducibility would be due to the fact that the presence of a large number of pure detergent micelles prevents a specific assembly of protein–detergent complexes. Thus, it was shown that detergent concentration just above the CMC is beneficial to the reproducibility of crystallization of a protein–detergent complex.

3.4. Precipitation solubility of integral membrane proteins solubilized in different types of detergents

To ascertain the influence of detergent type on the solubility of a protein–detergent complex, precipitate curves were determined for *Rb. sphaeroides* RC and B800–850 solubilized in different types of detergent. Part of the precipitate curves obtained for *Rb. sphaeroides* RC using PEG4000 and $(NH_4)_2SO_4$ as a precipitant are shown in Fig. 6A and B, respectively. With an increase in PEG4000 concentration, this protein solubilized in Brij-35 began to precipitate just above 31% (w/v), and the precipitate solubility in other detergents showed a steep exponential decrease. Depending on the detergent type, in particular the properties of the hydrophilic head, the precipitate curve shifted toward the lower PEG4000 concentration in the order $C_{12}E_8$, Triton X-100, LDAO, MEGA-9, decanoyl-*n*-methylglucamide (MEGA-10, Dojindo), OG, NTM, OTG, DM, LM, SM-1200, SM-1000 and *n*-heptyl-β-D-thioglucoside (HTG, Dojindo). On the other hand, the precipitate curve of *Rb. sphaeroides* B800–850 shifted in the order Triton X-100, $C_{12}E_8$, DDAO, LDAO, OG, SM-1200, NTM, OTG, DM, LM, MEGA-9 and MEGA-10. Although both proteins differ in isoelectric point and molecular weight, the

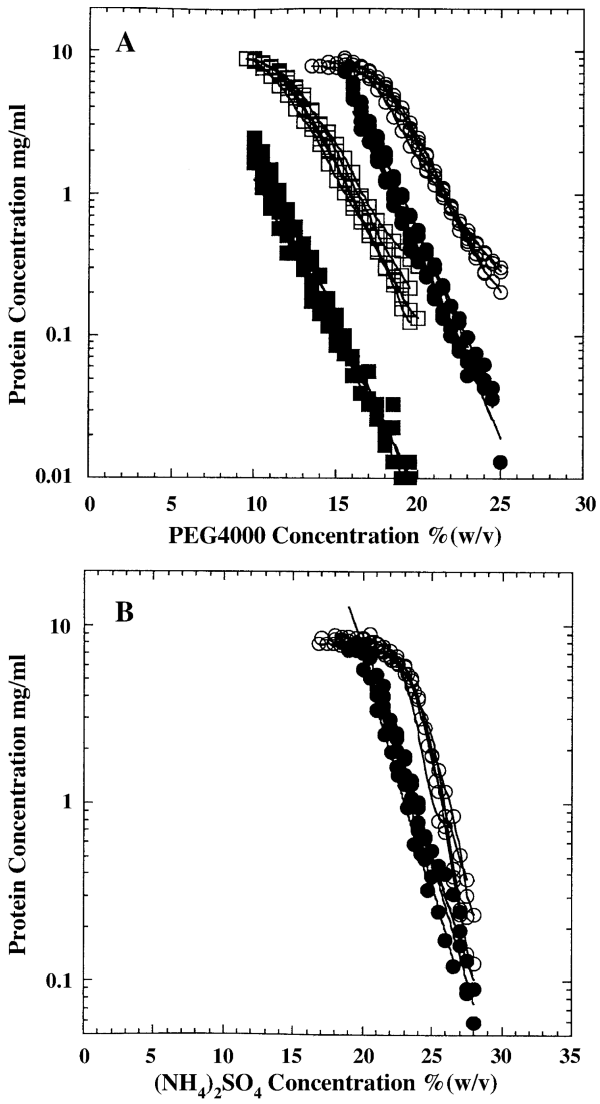

Fig. 5. The effect of detergent concentration on the solubility of an amorphous precipitate and a crystal of *Rb. sphaeroides* RC and *Rp. viridis* RC. For *Rb. sphaeroides* RC (A) and *Rp. viridis* RC (B), the protein concentration in the supernatant at room temperature (21–24 °C) immediately after removing amorphous precipitates (open symbol) and crystals (closed symbol) by centrifugation was plotted as a function of PEG4000 and $(NH_4)_2SO_4$ in a semi-logarithmic way, respectively. The concentrations of LDAO (○): were 0.1%, 0.5%, 1.0%, 1.5% and 2.0% (w/v). The concentrations of OG (□): were 0.8%, 1.0%, 1.6%, 2.4% and 3.2% (w/v). For *Rb. sphaeroides* RC, the other conditions were: 10 mM Tris–HCl (pH 8.0), 1 mM EDTA-2Na$^+$, 0.02% (w/v) NaN_3 and 300 mM NaCl. For *Rp. viridis* RC, the other conditions were: 100 mM sodium phosphate (pH 7.0), 3% (w/v) triethylammonium phosphate, 3% (w/v) heptane-1,2,3-triol, 0.02% (w/v) NaN_3 and 1 mM EDTA-2Na$^+$.

order of oligooxyethilene, *N*,*N*-dimethyl-amine-*N*-oxide, monosaccharide and disaccharide hydrophilic head detergents was common to both proteins except in the case of methylglucamide. Such a tendency is ascribed to the competition of the hydrophilic head with PEG4000 for water molecules. Moreover, the slope of precipitate curves gradually steepened with the shift toward lower PEG4000 concentration.

Precipitate solubility of all the other complexes except *Rb. sphaeroides* B800–850/Triton X-100 complex decreased in a single exponential way with an increase in $(NH_4)_2SO_4$ concentration as well as PEG4000. The slope also gradually steepened with the shift toward lower $(NH_4)_2SO_4$ concentration. With respect to the detergent type, however, the sequence of precipitate curves differed

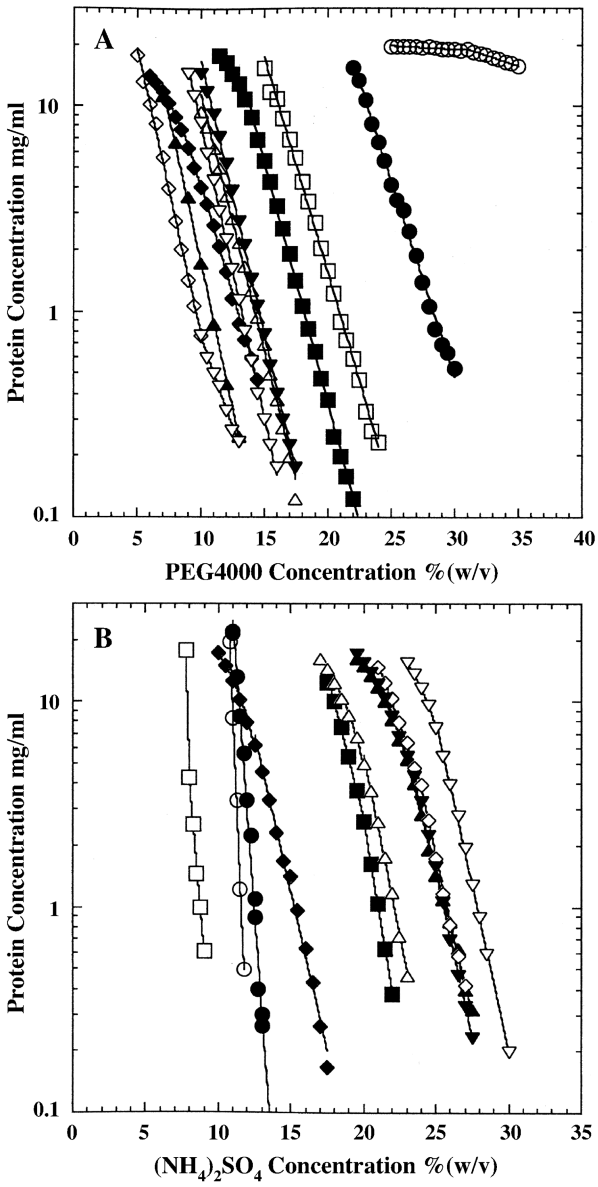

Fig. 6. Precipitate solubility of *Rb. sphaeroides* RC solubilized in different detergents as a function of precipitant concentration in a semi-logarithmic way. The precipitants used were: PEG4000 (A) and $(NH_4)_2SO_4$ (B). Symbols are the protein concentrations remaining in the supernatant at room temperature (21–24 °C) immediately after removing an amorphous precipitate by centrifugation. The concentrations and types of solubilization detergents were: 0.1% (w/v) Brij-35 (○), 0.1% (w/v) $C_{12}E_8$ (●), 0.1% (w/v) Triton X-100 (□), 0.1% (w/v) LDAO (■), 0.8% (w/v) OG (△), 0.1% (w/v) LM (▲), 0.1% (w/v) SM-1200 (◇), 0.3% (w/v) OTG (◆), 0.2% (w/v) NTG (▽), and 0.9% (w/v) MEGA-9 (▼). The other conditions were: 10 mM Tris–HCl (pH 8.0), 1 mM EDTA-2Na$^+$, 0.02% (w/v) NaN_3 and 300 mM NaCl.

from that in PEG4000 as follows: (i) precipitate curves of *Rb. sphaeroides* RC shifted toward the lower $(NH_4)_2SO_4$ concentration in the order NTM, SM-1200, MEGA-9, LM, OG, LDAO, OTG, $C_{12}E_8$, Brij-35 and Triton X-100; and (ii) for *Rb. sphaeroides* 800–850, the detergent sequence was NTM, MEGA-9, OG, LDAO, LM, SM-1200, OTG, $C_{12}E_8$ and Triton X-100. Both proteins solubilized in oligooxyethilene head detergents precipitated at rather low $(NH_4)_2SO_4$ concentration, which would be due to the property of ethylene in the detergent head. In addition, the regularity seen in PEG4000 was not recognized with respect to the sequence of other detergents. This would be ascribed to the particularity in $(NH_4)_2SO_4$–detergent interactions at fairly high $(NH_4)_2SO_4$ concentration.

3.5. Precipitate solubility of different integral membrane proteins solubilized in LM

To establish how the precipitate solubility of a complex is related to the physical and chemical properties of a protein, precipitate curves were determined for five different integral membrane proteins solubilized in LM using PEG4000 and $(NH_4)_2SO_4$ as a precipitant (Fig. 7). Precipitate curves shifted toward the lower PEG4000 concentration in the order *Rb. sphaeroides* B800–850, *Rb. capsulatus* B800–850, *Rb. sphaeroides* RC, *Rp. viridis* RC and *Rp. viridis* RC-B1020. From their amino acid composition, isoelectric points of *Rb. capsulatus*, B800–850 [39], *Rb. sphaeroides* B800–850 [15] and RC [40], *Rp. viridis* RC [41–43] and RC-B1020 [44] are estimated to be 4.3–4.5, 4.0–4.3, 6.3, 8.0–8.2 and 8.2–8.6, respectively. The sequence on the protein type corresponds well with the relationship between the difference in the isoelectric point of each protein to pH of the solvent. Furthermore, from their tertiary structure [25,45–47] and retention time by molecular sieve chromatography on CL-6B, the order of molecular weight is *Rb. sphaeroides* RC < *Rp. viridis* RC < *Rb. capsulatus* B800–850, *Rb. sphaeroides* B800–850 < *Rp. viridis* RC-B1020. The slopes of the precipitate curves steepened in this order. However, clear exponential dependence of the slope on the molecular weight seen in aqueous-soluble proteins [31] was not shown between the molecular weight of those proteins and the slope of the precipitate curve. This is ascribed to the extensive distribution of the amount of detergent binding to the proteins.

Rb. capsulatus B800–850 did not precipitate up to 30% (w/v) $(NH_4)_2SO_4$. Precipitate curves of the other proteins shifted toward lower $(NH_4)_2SO_4$ concentration in the order *Rp. viridis* RC-B1020, *Rb. sphaeroides* B800–850, *Rb. sphaeroides* RC and *Rp. viridis* RC, and the slope steepened in the order *Rb. sphaeroides* B800–850, *Rb. sphaeroides* RC, *Rp. viridis* RC and *Rp. viridis* RC-B1020. The regularity seen in PEG4000 was also not shown with respect to the sequence of proteins. This would also be ascribed to the particularity in $(NH_4)_2SO_4$–protein interactions at fairly high $(NH_4)_2SO_4$ concentration.

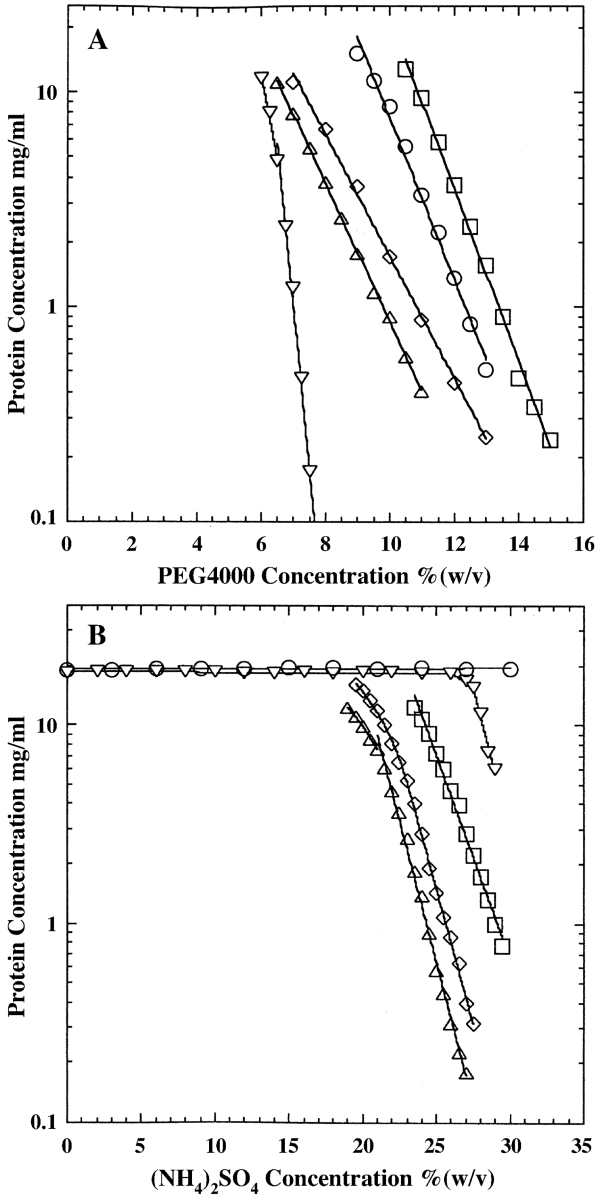

Fig. 7. Precipitate solubility of different integral membrane proteins solubilized in LM in a semi-logarithmic way. The precipitants used were: PEG4000 (A) and $(NH_4)_2SO_4$ (B). Symbols are the protein concentrations remaining in the supernatant at room temperature (21–24 °C) immediately after removing an amorphous precipitate by centrifugation. Proteins were: *Rb. capsulatus* B800–850 (○), *Rb. sphaeroides* B800–850 (□), *Rb. sphaeroides* RC (◇), *Rp. viridis* RC (△) and *Rp. viridis* RC-B1020 (▽). The other conditions were: 25 mM Tris–HCl (pH 8.0), 1 mM EDTA-$2Na^+$, 0.02% (w/v) NaN_3.

4. Discussion

Detergents to maintain a target protein in its natural conformation should be determined at the first step of a crystallization trial because a high-quality crystal suitable

for X-ray crystallography is never formed from denatured or structurally heterogeneous proteins. From the stability of several integral membrane proteins, it was shown that the influence of detergents on protein conformation increases with an increase in their own flexibility, an increase in the polarity and a decrease in the size of their hydrophilic head. This feature corresponds well with results from the thermal stability of rhodopsin and opsin [21,26]. In addition, a 10-carbon alkyl tail detergent was the most advantageous for the stability of *Rp. viridis* RC-B1020 among those with the same hydrophilic head. For the major fatty acid composition (16 and 18 carbon atoms) of *Rp. viridis* photosynthetic membrane [48], this length is reasonable from the viewpoint of stereochemistry as follows. In order to pack the tails moderately within the hemispherical micelle core so as to maintain both interactions of detergent heads with polar amino acid side chains corresponding to the membrane surface and of detergent hydrophobic tails with hydrophobic amino acid side chains, the length of the alkyl tail must be shorter by 20–25% than that of the lipid. In addition, the minimum dimension of micelles, which may have a spherical, rod or disc shape, exceeds twice the all-trans length of the molecules by 10–30% [49]. Therefore, the suitable length for an alkyl chain would be within the range of 8–14 carbon atoms corresponding to the fatty acid composition normally varying from 14 to 24 carbon atoms [48]. Probably, the conclusion in the previous study that detergents are milder the longer their hydrophobic tail [21,26] is owing to the temperature dependence characteristic of hydrophobic interaction. Thus, the influence of detergent type on a protein is related to chemical and physical properties of a detergent, although there is certainly particularity in the influence.

For the orderly arrangement of protein–detergent complexes in a crystal, a detergent micelle surrounding a protein should be small and easily change its shape so as to allow the protein–protein-specific interactions [1]. However, such small and flexible detergents usually strongly influence the activity and conformation of integral membrane proteins. Given such a dilemma, we must test the stability of a target protein. In this case, it is sufficient only to examine five detergents with different hydrophilic heads (LDAO, $C_{12}E_8$, MEGA-9, OG and LM, for example), because suitable alkyl tail length can be estimated from major fatty acid composition of the source. This stability check leads to a reasonable choice of other suitable detergents by referring to the discussion above or the sequence shown in Table 2. From crystallization trials of several integral membrane proteins in our laboratory, a criterion of detergent choice is whether or not more than 90% of a target protein is stable after a week. Among the candidates limited in this way, smaller and more flexible detergents should be preferentially used for the crystallization experiments. Moreover, because slightly higher detergent concentration above the CMC is advantageous to the reproducibility of crystallization, apart from crystal size, it is not necessary to test various detergent concentrations in an initial crystallization trial. Thus, the number of possible combinations of detergent type and concentration can be largely reduced.

Crystal formation is difficult in an integral membrane protein solubilized in steroidal detergents because of the bulky, rigid and inhomogeneous property of its micelles [21]. However, steroidal detergents are useful for solubilization and purification because the denaturation and inactivation of many integral membrane proteins are reduced. In a crystallization trial, steroidal detergents must be finally replaced with other detergents suitable for crystallization taking into account the concentration of the replacement detergent as shown in this study.

To appreciate the relationship between protein solubility and precipitant concentration suitable for crystallization, solubility diagrams were determined for four different protein–detergent complexes. In all cases, the solubility of an amorphous precipitate was higher than that of a crystal at the same precipitant concentration, and the slope of the precipitate curve was the same as, or less steep than that of the solubility curve. These two relationships reflect well a requirement that the crystallization of a protein–detergent complex is induced by predominant interactions between specific sites on a protein.

As shown in Fig. 8, the consideration of crystal growth based on the two relationships provides a deeper insight into the choice of suitable precipitant concentration. Because the degree of supersaturation increases with an increase in precipitant concentration, there is a minimum precipitant concentration to induce the nucleation of a protein crystal. Within such a limited range of precipitant concentration, the difference between precipitate and crystal solubilities, the amount of a complex converted to a crystalline phase, decreases with an increase in precipitant concentration. To make protein molecules participate in the crystalline phase as much as possible, therefore, a low precipitant concentration within the range corresponding to the large decrease in the precipitate solubility should be chosen. This corresponds well with a well-known empirical rule that precipitant concentration yielding a slight protein precipitate is suitable for its crystallization in a batch experiment [7].

In a vapor diffusion experiment, a considerably high precipitant concentration of a reservoir solution forces the path of crystal growth (curve EG in Fig. 8) in the precipitation zone because of rapid water evaporation. On the contrary, when the precipitant concentration is set below the range where the precipitate solubility begins to largely decrease, sample solutions often cannot reach the nucleation zone. In addition, a small difference in precipitant concentration between sample and reservoir solutions reduces an unfavorable increase in the detergent concentration. Therefore, suitable initial conditions of the sample solution and the reservoir are precipitant concentrations where precipitate solubility begins to decrease largely for a given protein concentration and crystal solubility is around zero, respectively.

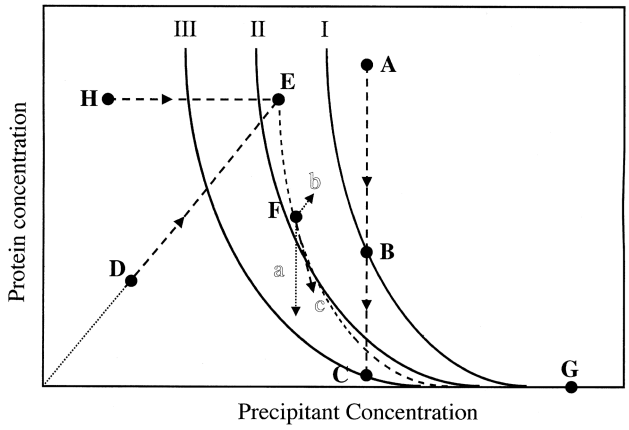

Fig. 8. Schematic solubility diagram representing correlation between protein and precipitating agent. The vertical and the horizontal axes represent the protein and the precipitant concentration, respectively. Curve I represents a precipitate curve on which the concentration of protein in a solution phase is defined as precipitate solubility at each precipitant concentration in this study. Curve III represents a solubility curve on which the concentration of protein in a solution at equilibrium with the crystal phase is defined as the crystal solubility at each precipitant concentration. The only protein in the zone between curves I and III can be used for crystallization. In addition, this zone is divided into two further zones for nucleation and growth and growth only of a protein crystal. Lines ABC, DEFG and HEFG represent the crystallization pathways on the batch, vapor diffusion and dialysis methods, respectively. When the initial condition of a sample solution (the combination of protein concentration and precipitant concentration) is set at point A, for example, in a batch experiment, since an excessive amount of protein separates as an amorphous precipitate from the solution, the concentration of protein soluble in the solution immediately falls at point B on the precipitate curve. When the combination of chemicals, temperature and pH is suitable for crystallization, the protein concentration in a solution decreases toward point C on the solubility curve with the crystal growth. When initial conditions of sample and reservoir solutions are set at points D and G in a vapor diffusion experiment, respectively, the protein and precipitant concentration in a sample solution first increase, maintaining the same ratio along line AB, and passing through the origin, during the evaporation of water. When the solution condition enters the nucleation zone, the nucleation of protein crystals begins at point F, for example. At this stage, since the conversion of protein molecules from a solution phase to a crystalline phase and the evaporation of water progress simultaneously, the solution condition is expected to change along curve EG. At point F on curve EG, the direction (𝕔) of the path of the sample condition is determined both by the evaporation rate of water (𝕒) and the driving force originating from the degree of supersaturation (𝕓). Here, the amplitude of 𝕒 is mainly proportional to the difference in the precipitant concentration at points F and G, and that of 𝕓 the ratio of the protein concentration at point F to the crystal solubility at the same precipitant concentration.

Phase separation [32] was observed for *Rb. sphaeroides* RC and *Rb. capsulatus* B800–850. For an accurate discussion, it necessary to introduce a time-axis to the schematic solubility diagram of Fig. 8, and then to consider the crystal growth using protein concentration in the protein-rich phase instead of precipitate solubility. Since the phase separation is induced from the supernatant solution, the protein concentration in both phases must have a particular relationship to the precipitate solubility. In addition, the total amount of the complex that is finally converted to a crystalline phase only depends on the difference between the precipitate and the crystal solubilities independently of the phase separation. Even in case of phase separation, therefore, precipitate solubility defined in this study provides useful information to reflect the crystallization quantitatively.

The good reproducibility of precipitate solubility requires consistency of protein purity, chemical solution, precise temperature control, and preparation of supernatant solution. As shown in Fig. 9, fortunately, suitable precipitant concentration is easily estimated from the minimum precipitant concentration to yield a protein precipitate for a given protein concentration instead of other notorious determinations of precipitate solubility. With the addition of precipitant solution, an amorphous precipitate usually begins to form at a precipitant concentration lower by 2–3% (w/v) than a precipitate curve for 5–10 mg/ml of protein concentration. Therefore, a precipitant concentration higher by 2–3% (w/v) than the minimum concentration is suitable in the batch experiment. In addition, the decrease in precipitate solubility from 10 to 1 mg/ml corresponds the increase in precipitant concentration of 5–6% (w/v) in many cases, and precipitate solubility is higher than corresponding crystal solubility

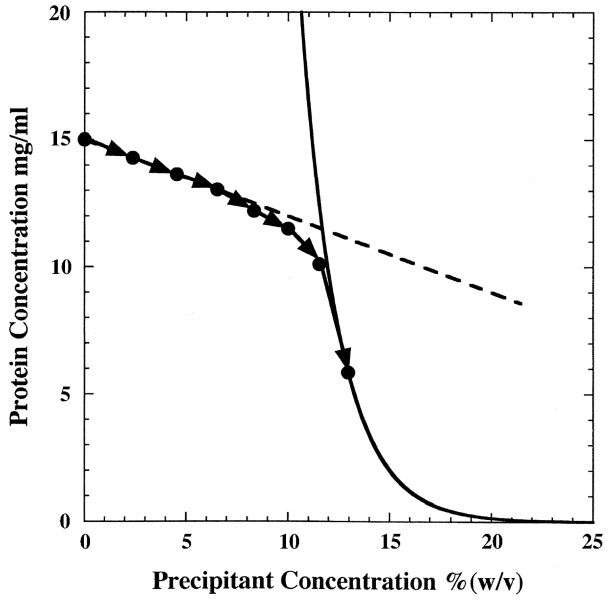

Fig. 9. Schematic solubility diagram representing experimental procedure to determine precipitant concentration suitable for batch and vapor diffusion experiments. The concentration of a targeted protein is adjusted to about 15 mg/ml because its final concentration of 5–10 mg/ml is usually suitable for crystallization. The condition change of a sample solution is represented as closed circles in the case that 50% (w/v) precipitant solution is added stepwise to 20 μl of the protein solution μl by μl, mixing until a slight protein precipitate is observed. A slight amorphous precipitate usually begins to form at a precipitant concentration lower by 2–3% (w/v) than the crossing of the trace of the sample solution above and the precipitate curve. In the batch experiment, a moderate precipitant concentration is higher by 2–3% (w/v) than this cloud point. In the vapor diffusion experiment, the moderate initial condition of a sample solution is exactly this cloud point and a moderate precipitant concentration of a reservoir solution is higher by 5–6% (w/v) than the cloud point.

under the crystallization conditions. In the vapor diffusion experiment, therefore, moderate initial precipitant concentrations of sample and reservoir solutions are exact and higher by 5–6% (w/v) than the cloud point, respectively.

When using the combination of PEG4000 and NaCl as a precipitant, the precipitate curve of protein–detergent complexes shifted, reflecting the physicochemical properties of detergent head. Salt usually eliminates net charges on the surface of a complex at low concentrations below 400 mM. PEG4000 added to such an aqueous solution competes with the complex for water molecules [50,51], so that the repulsive short-range hydration force between the complex surfaces is reduced. On the other hand, a further increase in salt concentration enhances local hydrophobic interaction between complexes [51–53] because of high polarity of bulk solvent on all sides of a protein–detergent complex. Polarity on the complex surface being between PEG4000 and $(NH_4)_2SO_4$ accounts for the reverse detergent-sequence of the precipitate curve against both precipitants. Furthermore, in the case of $(NH_4)_2SO_4$, less regularity was shown for the relationship between the behavior of the precipitate curve and detergent type or protein property. This may be ascribed to the small ratio of hydrophobic amino acid in the extramembraneous regions and the influence of high salt concentration on detergent micelles.

To easily determine crystallization conditions of a targeted protein, it is necessary to know the dependence of precipitate solubility on the factors above in advance. Knowledge of the detergent-related phenomena shown in this study would also be useful for the preparation and crystallization of other integral membrane proteins. To further limit the range to be tested, it is necessary to know the influence of other factors such as properties of salt and precipitant, temperature and pH on precipitate solubility. We will show useful features common to such influence in detail in a series of studies after this.

Acknowledgements

We are grateful to Dr. Gebhard F.X. Schertler of MRC Laboratory of Molecular Biology, Dr. Tatsuo Katsura and Dr. Kazuaki Harata of AIST for their useful suggestion, and Director Yoshimasa Kyougoku of BIRC AIST (who unfortunately passed away on February 26, 2003) for his moral support. This work was partly supported by a STA-COE grant to the author. The data collection was performed with the approval of the Photon Factory Advisory Committee (Proposal No. 99P009).

References

[1] R.M. Garavito, Z. Markovic-Housley, J.A. Jenkins, The growth and characterization of membrane protein crystals, J. Cryst. Growth 76 (1986) 701–709.
[2] R.M. Garavito, D. Picot, P.J. Loll, Strategies for crystallizing membrane proteins, J. Bioenerg. Biomembranes 28 (1996) 13–27.
[3] H. Michel, D. Oesterhelt, Three-dimensional crystals of membrane proteins: bacteriorhodopsin, Proc. Natl. Acad. Sci. U. S. A. 77 (1980) 1283–1285.
[4] R.M. Garavito, J.P. Rosenbush, Three-dimensional crystals of an integral membrane protein, J. Cell Biol. 86 (1980) 327–329.
[5] M. Tanaka, H. Suzuki, T. Ozawa, The crystallization of mitochondrial cytochrome oxidase–cytochrome *c* complex, Biochim. Biophys. Acta 612 (1980) 295–298.
[6] T. Ozawa, M. Tanaka, Y. Shimomura, Crystallization of the middle part of the mitochondrial electron transfer chain: cytochrome bc_1–cytochrome *c* complex, Proc. Natl. Acad. Sci. U. S. A. 77 (1980) 5084–5086.
[7] A. McPherson, Current approaches to macromolecular crystallization, Eur. J. Biochem. 189 (1990) 1–23.
[8] J. Jancarik, S.-H. Kim, Sparse matrix sampling: a screening method for crystallization of proteins, J. Appl. Crystallogr. 24 (1991) 409–411.
[9] G. Feher, Z. Kam, Nucleation and growth of protein crystals: general principles and assays, Methods Enzymol. 114 (1985) 77–112.
[10] M. Ries-Kautt, A. Ducruix, Phase diagram, in: A. Ducruix, R. Giegé (Eds.), Crystallization of Nucleic Acids and Proteins: A Practical Approach, IRL Press, Oxford, 1992, pp. 195–218.
[11] T. Odahara, M. Ataka, T. Katsura, Phase diagram determination to elucidate the crystal growth of the photoreaction center from *Rhodobacter sphaeroides*, Acta Crystallogr., D Biol. Crystallogr. 50 (1994) 639–642.
[12] J.-F. Gaucher, M. Riés-Kautt, F. Reiss-Husson, A. Ducruix, Solubility diagram of *Rhodobacter sphaeroides* reaction center as a function of PEG concentration, FEBS Lett. 401 (1997) 113–116.
[13] R.K. Clayton, B.J. Clayton, Molar extinction coefficients and other properties of an improved reaction center preparation from *Rhodopseudomonas viridis*, Biochim. Biophys. Acta 501 (1978) 478–487.
[14] H.A. Frank, S.S. Taremi, J.R. Knox, Crystallization and preliminary X-ray and optical spectroscopic characterization of the photochemical reaction center from *Rhodobacter sphaeroides* strain 2.4.1, J. Mol. Biol. 198 (1987) 139–141.
[15] R.J. Cogdell, J.G. Lindsay, G.P. Reid, G.D. Webster, A comparison of the constituent polypeptides of the B-800–850 light-harvesting pigment–protein complex from *Rhodopseudomonas sphaeroides*, Biochim. Biophys. Acta 591 (1980) 312–320.
[16] R.J. Cogdell, K.J. Woolley, L.A. Ferguson, D.J. Dawkins, Crystallization of purple bacterial antenna complexes, in: H. Michel (Ed.), Crystallization of Membrane Proteins, CRC Press, Boca Raton, FL, 1991, pp. 125–136.
[17] W. Welte, T. Wacker, M. Leis, W. Kreutz, J. Shiozawa, J. Gad'on, G. Drews, Crystallization of the photosynthetic light-harvesting pigment–protein complex B800–850 *Rhodopseudomonas capsulata*, FEBS Lett. 182 (1985) 260–264.
[18] M. Hara, K. Namba, Y. Hirata, T. Majima, S. Kawamura, Y. Asada, J. Miyake, The photoreaction unit in *Rhodopseudomonas viridis*, Plant Cell Physiol. 31 (1990) 951–960.
[19] T. Ueda, Y. Morimoto, M. Sato, T. Kakuno, J. Yamashita, T. Horio, Isolation, characterization, and comparison of a ubiquitous pigment–protein complex consisting of a reaction center and light-harvesting bacteriochlorophyll proteins present in purple photosynthetic bacteria, J. Biochem. 98 (1985) 1487–1498.
[20] J.P. Allen, G. Feher, Crystallization of reaction center from *Rhodopseudomonas sphaeroides*: preliminary characterization, Proc. Natl. Acad. Sci. U. S. A. 81 (1984) 4795–4799.
[21] W. Külbrandt, Three-dimensional crystallization of membrane proteins, Q. Rev. Biophys. 21 (1988) 429–477.
[22] N. Sakabe, A focusing Weissenberg camera with multi-layer-line screens for macromolecular crystallography, J. Appl. Crystallogr. 16 (1983) 542–547.
[23] Z. Otwinowski, W. Minor, Data collection and processing, in: L. Sawyer, N. Isaacs, S. Bailey (Eds.), Proc. CCP4 Study Weekend,

29–30 Jan. 1993, SERC Daresbury Laboratory, Warrington, 1993, pp. 56–62.
[24] S. Karrasch, P.A. Bullough, R. Ghosh, The 8.5 Å projection map of the light-harvesting complex I from *Rhodospirillum rubrum* reveals a ring composed of 16 subunits, EMBO J. 14 (1995) 631–638.
[25] I. Ikeda-Yamasaki, T. Odahara, K. Mitsuoka, Y. Fujiyoshi, K. Murata, Projection map of the reaction center–light harvesting 1 complex from *Rhodopsedomonas viridis* at 10 Å resolution, FEBS Lett. 425 (1998) 505–508.
[26] W. DeGrip, Thermal stability of rhodopsin and opsin in some novel detergents, Methods Enzymol. 81 (1982) 256–265.
[27] H. Michel, Three-dimensional crystals of a membrane protein complex, J. Mol. Biol. 158 (1982) 567–572.
[28] C.-H. Chang, M. Schiffer, D. Tiede, U. Smith, J. Noriss, Characterization of bacterial photosynthetic reaction center crystals from *Rhodopseudomonas sphaeroides* R-26 by X-ray diffraction, J. Mol. Biol. 186 (1985) 201–203.
[29] J.P. Allen, G. Feher, T.O. Yeates, D.C. Rees, J. Deisenhofer, H. Michel, R. Huber, Structural homology of reaction centers from *Rhodopseudomonas sphaeroides* and *Rhodopseudomonas viridis* as determined by X-ray diffraction, Proc. Natl. Acad. Sci. U. S. A. 83 (1986) 8589–8593.
[30] A. Ducruix, F. Reiss-Husson, Preliminary characterization by X-ray diffraction of crystals of photochemical reaction centres from wild-type *Rhodopseudomonas sphaeroides*, J. Mol. Biol. 193 (1987) 419–421.
[31] I.R.M. Juckes, Fraction of proteins and viruses with polyethylene glycol, Biochim. Biophys. Acta 229 (1971) 535–546.
[32] W. Welte, T. Wacker, Protein–detergent micellar solutions for the crystallization of membrane proteins: some general approaches and experiences with the crystallization of pigment–protein complexes from purple bacteria, in: H. Michel (Ed.), Crystallization of Membrane Proteins, CRC Press, Boca Raton, FL, 1991, pp. 107–123.
[33] C.-H. Chang, D. Tiede, J. Tang, U. Smith, J. Noriss, M. Schiffer, Structure of *Rhodopseudomonas sphaeroides* R-26 reaction center, FEBS Lett. 205 (1986) 82–86.
[34] S.D. Durbin, G. Feher, Studies of crystal growth mechanisms of proteins by electron microscopy, J. Mol. Biol. 212 (1990) 763–774.
[35] P.C. Weber, Physical principles of protein crystallization, Adv. Protein Chem. 41 (1991) 1–36.
[36] Y. Bessho, M. Ataka, M. Asai, T. Katsura, Analysis of the crystallization kinetics of lysozyme using a model with polynuclear growth mechanism, Biophys. J. 66 (1994) 310–313.
[37] V. Mikol, J.-L. Rodeau, R. Giegé, Changes of pH during biomacromolecule crystallization by vapor diffusion using ammonium sulfate as the precipitant, J. Appl. Crystallogr. 22 (1989) 155–161.
[38] A. Ducruix, R. Giegé, Methods of crystallization, in: A. Ducruix, R. Giegé (Eds.), Crystallization of Nucleic Acids and Proteins: A Practical Approach, IRL Press, Oxford, 1992, pp. 73–98.
[39] J.A. Shiozawa, P.A. Cuendet, G. Drews, H. Zuber, Isolation and characterization of the polypeptide components from light-harvesting pigment–protein complex B800–850 of *Rhodopseudomonas capsulata*, Eur. J. Biochem. 111 (1980) 455–460.
[40] J.C. Williams, L.A. Steiner, G. Feher, Primary structure of the reaction center from *Rhodopseudomonas sphaeroides*, Proteins 1 (1986) 321–325.
[41] H. Michel, K.A. Weyer, H. Gruenberg, F. Lottspeich, The 'heavy' subunit of the photosynthetic reaction center from *Rhodospeudomonas viridis*: isolation of the gene, nucleotide and amino acid sequence, EMBO J. 4 (1985) 1667–1672.
[42] H. Michel, K.A. Weyer, H. Gruenberg, I. Dunger, D. Oesterhelt, F. Lottspeich, The 'light' and 'medium' subunits of the photosynthetic reaction center from *Rhodopseudomonas viridis*: isolation of the genes, nucleotide and amino acid sequence, EMBO J. 5 (1986) 1149–1158.
[43] K.A. Weyer, F. Lottspeich, H. Gruenberg, F. Lang, D. Oesterhelt, H. Michel, Amino acid sequence of the cytochrome subunit of the photosynthetic reaction centre from the purple bacterium *Rhodopseudomonas viridis*, EMBO J. 6 (1987) 2197–2202.
[44] R.A. Brunisholz, F. Jay, F. Suter, H. Zuber, The light-harvesting polypeptides of *Rhodopseudomonas viridis*: the complete amino acid sequences of B1015-α, B1015-β and B1015-γ, Biol. Chem. Hoppe-Seyler 366 (1985) 87–98.
[45] J. Deisenhofer, O. Epp, K. Miki, R. Huber, H. Michel, X-ray structure analysis of a membrane protein complex: electron density map at 3 Å resolution and a model of the chromophores of the photosynthetic reaction center from *Rhodopseudomonas viridis*, J. Mol. Biol. 180 (1984) 385–398.
[46] J.P. Allen, G. Feher, T.O. Yeates, H. Komiya, D.C. Ress, Structure of the reaction center from *Rhodobacter sphaeroides* R-26: the protein subunits, Proc. Natl. Acad. Sci. U. S. A. 84 (1987) 6162–6166.
[47] G. McDermott, S.M. Prince, A.A. Freer, A.M. Hawthornthwaite-Lawless, M.Z. Papiz, R.J. Cogdell, N.W. Isaacs, Crystal structure of an integral membrane light-harvesting complex from photosynthetic bacteria, Nature 374 (1995) 517–521.
[48] P.F. Smith, Archaebacteria and other specialized bacteria, in: C. Ratledge, S.G. Wilkinson (Eds.), Microbial Lipids, vol. 1. Academic Press, Tokyo, 1988, pp. 489–553.
[49] M. Zulauf, Detergent phenomena in membrane protein crystallization, in: H. Michel (Ed.), Crystallization of Membrane Proteins, CRC Press, Boca Raton, FL, 1991, pp. 53–72.
[50] J.C. Lee, L.L.Y. Lee, Preferential solvent interactions between proteins and polyethylene glycol, J. Biol. Chem. 256 (1981) 625–631.
[51] T. Arakawa, S.N. Timasheff, Theory of protein solubility, Methods Enzymol. 114 (1985) 49–77.
[52] A.A. Green, Studies in the physical chemistry of the proteins: X. The solubility of hemoglobin in solutions of chlorides and sulfates of varying concentration, J. Biol. Chem. 95 (1932) 47–66.
[53] W. Melander, C. Horvath, Salt effects on hydrophobic interactions in precipitation and chromatography of proteins: an interpretation of the lyotropic series, Arch. Biochem. Biophys. 183 (1977) 200–215.